How to cite: *Angew. Chem. Int. Ed.* **2023**, *62*, e202303233
doi.org/10.1002/anie.202303233

CO_2 Reduction Reaction | Hot Paper

Molecular Engineering of Cation Solvation Structure for Highly Selective Carbon Dioxide Electroreduction

*Wenpeng Ni[+], Yongji Guan[+], Houjun Chen, Yan Zhang, Shuangyin Wang, and Shiguo Zhang**

Abstract: Balancing the activation of H_2O is crucial for highly selective CO_2 electroreduction (CO_2RR), as the protonation steps of CO_2RR require fast H_2O dissociation kinetics, while suppressing hydrogen evolution (HER) demands slow H_2O reduction. We herein proposed one molecular engineering strategy to regulate the H_2O activation using aprotic organic small molecules with high Gutmann donor number as a solvation shell regulator. These organic molecules occupy the first solvation shell of K^+ and accumulate in the electrical double layer, decreasing the H_2O density at the interface and the relative content of proton suppliers (free and coordinated H_2O), suppressing the HER. The adsorbed H_2O was stabilized via the second sphere effect and its dissociation was promoted by weakening the O–H bond, which accelerates the subsequent $*CO_2$ protonation kinetics and reduces the energy barrier. In the model electrolyte containing 5 M dimethyl sulfoxide (DMSO) as an additive (KCl-DMSO-5), the highest CO selectivity over Ag foil increased to 99.2 %, with FE_{CO} higher than 90.0 % within −0.75 to −1.15 V (vs. RHE). This molecular engineering strategy for cation solvation shell can be extended to other metal electrodes, such as Zn and Sn, and organic molecules like N,N-dimethylformamide.

Introduction

With decreasing the levelized cost of producing electricity from solar and wind power, renewables-powered electrolytic reduction of carbon dioxide (CO_2RR) in aqueous electrolytes holds great promise for the production of high-value chemicals.[1] In aqueous CO_2RR, the alkaline environment near the working electrode leads to H_2O molecules serving as the main source of protons for CO_2RR and the competing hydrogen evolution reaction (HER). This creates a conflict, as the proton-electron coupled nature of CO_2RR necessitates efficient activation of H_2O and smooth proton transfer,[2] while simultaneously exhibiting sluggish activity in H_2O reduction to prevent HER. As a result, a carefully calibrated balance of H_2O activation at the interface is imperative for highly selective CO_2RR. Since the reactions occur at the electrode-electrolyte interface (EEI), optimizing the EEI microstructure is pivotal for balancing H_2O dissociation by manipulating interfacial properties such as surface charge density, interface electric field strength, and local pH.[3]

Under the bias below the zero-charge potential, the EEI microstructure could be defined by the electric double layer (EDL) consisting of the inner Helmholtz plane (IHP) and the outer Helmholtz plane (OHP). The regulation of the structure and composition of IHP and OHP is prominent in modulating the state and reactivity of the interfacial H_2O molecules.[4] For example, specifically adsorbed surfactant in IHP undergoes a dynamic assembly process that repels isolated water from the electrode and suppresses HER.[5] As for OHP, solvated cations reside in this layer, and the effects of metal cation identity and concentration have been well recognized.[6] Cations with smaller hydration shells are concentrated at the OHP and have a narrow gap between the electrode and OHP, giving larger surface charge density and stronger interfacial electric field.[7] The optimized electric field helps to suppress the migration of hydronium ions to the active sites, mitigating the activation of H_2O molecules.[8] The concentration effect is also essential, as a highly concentrated electrolyte exhibits strong solvation for metal cations, reducing the amount of free water and lowering proton availability.[9] Although these approaches have succeeded in depleting the activity of HER, they are not capable of simultaneously tuning the kinetic rates of protonation steps in CO_2RR.[10] Meanwhile, the limited types and solubility of surfactants and cations hinder their wide application. Further efforts should be pursued to create innovative and adaptable methods for regulating the activation of H_2O for both HER and CO_2RR in a balanced manner.

In this work, we present a molecular engineering strategy for a metal cation solvation sheath to regulate H_2O

[*] Dr. W. Ni,[+] H. Chen, Prof. Y. Zhang, Prof. S. Zhang
College of Materials Science and Engineering, Hunan University
Changsha 410004 (China)
E-mail: zhangsg@hnu.edu.cn
Prof. Y. Guan[+]
Institute of Optoelectronics and Electromagnetic Information, School of Information Science and Engineering, Lanzhou University
Lanzhou, 730000 (China)
Prof. S. Wang
State Key Laboratory of Chem/Bio-Sensing and Chemometrics, Advanced Catalytic Engineering Research Center of the Ministry of Education, College of Chemistry and Chemical Engineering, Hunan University
Changsha 410082 (China)
[+] These authors contributed equally to this work.

activation and improve CO_2RR selectivity, using aqueous electrolytes containing aprotic organic molecules with a higher Gutmann donor number than H_2O. These organic molecules are incorporated into the solvation shell of the cation and migrate to the OHP under the applied bias. The enrichment of these organic molecules at the interface modifies the state of the H_2O molecule in the EDL and interacts with adsorbed water ($*H_2O$), suppressing HER through thermodynamic regulation and promoting CO_2RR through kinetic modulation. The proof-of-concept using dimethyl sulfoxide (DMSO) within the K^+ solvation sheath over the Ag foil electrode showed enhanced CO_2-to-CO conversion. Molecular dynamics (MD) simulations and in situ attenuated total reflectance surface-enhanced infrared adsorption spectroscopy (ATR-SEIRAS) have demonstrated a marked decline in the density of H_2O molecules and the relative content of isolated and coordinated H_2O in proximity to the electrode. The presence of DMSO accelerates the dissociation of $*H_2O$ and promotes the protonation of $*CO_2$, lowering the energetic barrier for forming *COOH and leading to a balanced activation of H_2O for HER and CO_2RR. A CO selectivity greater than 90.0 % was achieved in the potential range of −0.75 to −1.15 V relative to RHE (all potentials henceforth are relative to RHE), and similar improvements in CO_2RR activity were observed for other organic additives and metal electrodes.

Results and Discussion

H_2O acts as the seesaw molecule to bifurcate the main reaction towards HER or CO_2RR. Considering that HER is typically dependent on proton source concentration in first-order relevance,[10] reducing the concentration of H_2O molecules within EDL may effectively inhibit H_2 evolution. This approach will not affect the activity of the active site for H_2O dissociation due to the electronic structure of the catalyst unchanged, thus maintaining the smooth protonation for CO_2RR. Therefore, we propose to partially replace the H_2O molecules in the cation solvation sheath with aprotic organic molecules that have good compatibility with water and sufficiently strong coordination ability toward the metal cation (Figure 1). These organic molecules incorporated cations could accumulate at the OHP under applied potentials and reduce the content of proton sources, suppressing HER via retarding the Volmer step or decreasing the coverage of *H. Moreover, these interfacial confined organic molecules can interact with $*H_2O$, thus spurring the kinetic rate of H_2O dissociation and enhancing CO_2RR activity. As an example, we choose DMSO as a molecular dopant for the solvation shell of K^+. The concentration of DMSO in the aqueous electrolyte can be adjusted over a wide range as DMSO is readily miscible with water in any ratio. More importantly, as indicated by its higher Gutmann donor number (29.8) compared to H_2O (18.0), DMSO theoretically has a preference for solvating with K^+.[11] Therefore, a model system containing 0.5 M KCl and 5 M DMSO (denoted as KCl-DMSO-5) was constructed to explore the feasibility of molecular engineering of the solvation structure for regulating the interfacial H_2O activation.

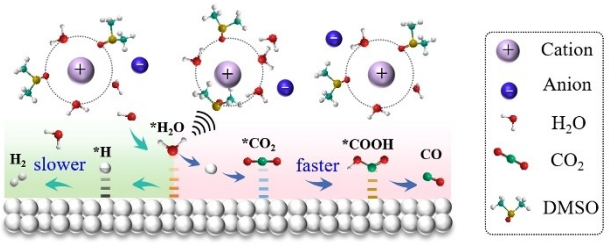

Figure 1. Molecular engineering strategy for cation solvation structure toward highly selective CO_2RR.

We first performed MD simulations to elucidate the microstructure of KCl-DMSO-5. The calculated density of this simulated system is 1.053 $g\,cm^{-3}$, which is very close to the experimental measurement (1.045 $g\,cm^{-3}$), confirming the reliability of the built model. The snapshot image depicts a homogeneously mixed system (Figure 2a), and the local structure analysis discloses that K^+ is surrounded by H_2O and DMSO molecules (Figures S1 and 2c). The radial distribution function (RDF) analysis reveals a characteristic peak of $K\text{-}O_{water}$ at 2.66 Å, which is attributed to the H_2O molecules in the first solvation shell of K^+ (Figure 2d). For DMSO, although the S and C atoms in the S=O and methyl moieties are far from K^+, a sharp peak of $K\text{-}O_{S=O}$ was observed with the same K–O distance as that of the $K\text{–}O_{water}$ pair. These results provide clear evidence of incorporating the DMSO molecule into the first solvation sheath of K^+ in KCl-DMSO-5. Considering that CH_3CN has a lower Gutmann donor number (14.1) than H_2O,[12] an electrolyte system containing 0.5 M KCl and 5 M acetonitrile (denoted as KCl-CH_3CN-5) was also constructed for comparative analysis (Figure 2b). According to the RDF analysis, N is the closest atom to K^+ among all the atoms in the CH_3CN molecule. However, the $K\text{–}N_{nitrile}$ is greater than the $K\text{–}O_{water}$, indicating that the primary coordination shell of K^+ predominantly consists of H_2O molecules (Figure 2e). As expected, CH_3CN does not occupy the solvation shell of K^+.

The dynamic evolution of the interfacial organic molecules was monitored using in situ ATR-SEIRAS, which captures accurate molecular information within a 5–10 nm range from the electrode surface.[13] As shown in Figures 2f and 2g, the characteristic peaks of the symmetric deformations of $–CH_3$ and stretching vibrations of S=O could be identified in N_2-saturated KCl-DMSO-5 (Figure S2), and their intensities increase gradually with the negative shift of applied potentials. This indicates that the DMSO molecules incorporated into the solvation shell of K^+ are enriched within the EDL. This is a reversible process (Figure S3). However, no peaks associated with the -CN group (2257 cm^{-1}, Figure S4) were observed in the KCl-CH_3CN-5 system at any potential (Figure 2h), as the CH_3CN molecules are freely distributed in the solution and do not migrate with K^+ under the electric field. The EDL capacitance was analyzed to further corroborate the locally enriched DMSO

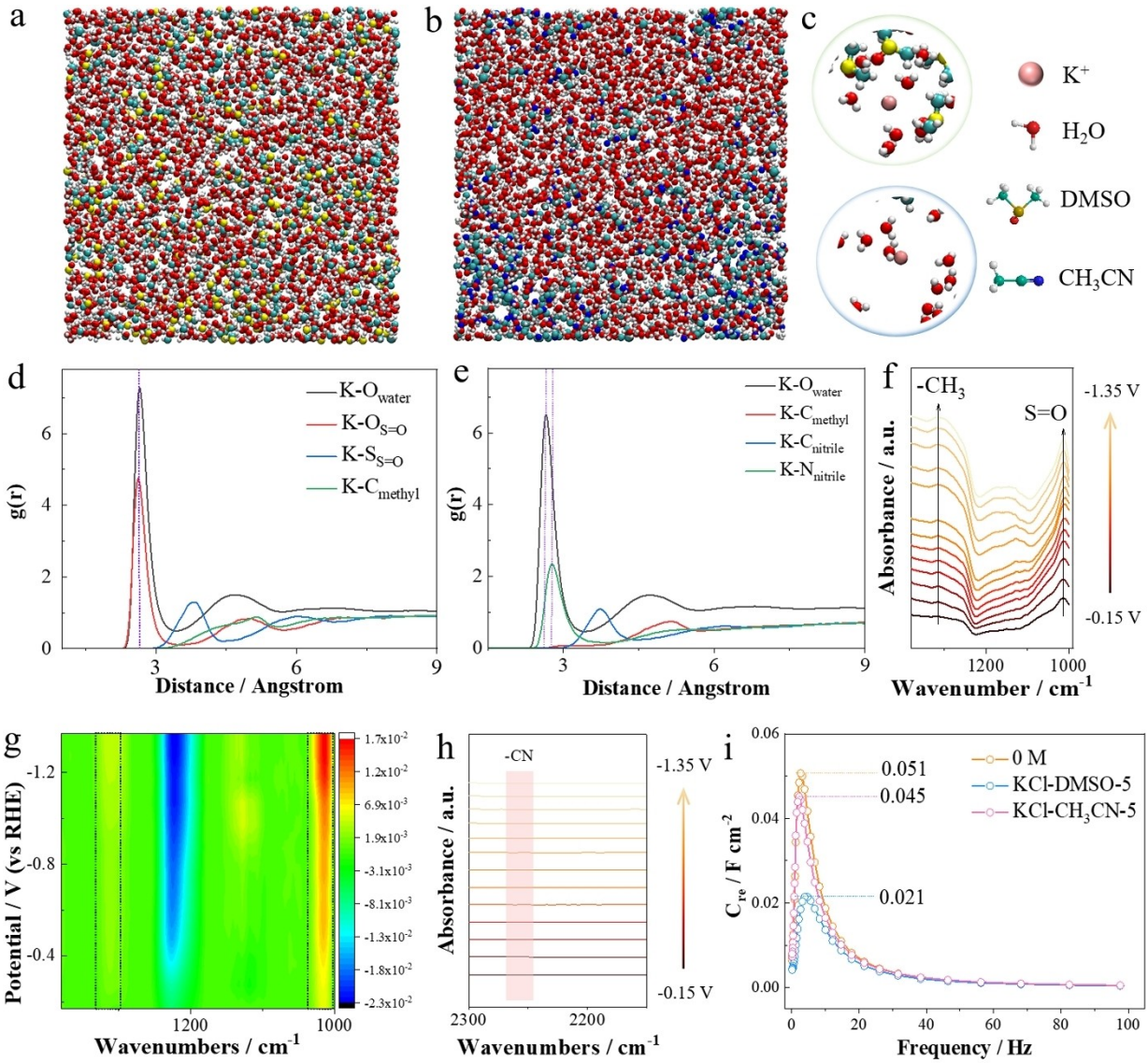

Figure 2. Characterization for electrolyte microstructure. Snapshots of (a) KCl-DMSO-5 and (b) KCl-CH_3CN-5 electrolyte molecular system obtained from MD simulation. Atom color coding: red: O, white: H, yellow: S, cyan: C, orange: K. (c) Local structure of KCl-DMSO-5 (top) and KCl-CH_3CN-5 (bottom) obtained from MD simulation. RDFs of (d) KCl-DMSO-5 and (e) KCl-CH_3CN-5. (f) In situ ATR-SEIRAS of the N_2-saturated KCl-DMSO-5 system in the range from 1000 to 1380 cm^{-1}, and (g) its corresponding contour image. (h) In situ ATR-SEIRAS of the N_2-saturated KCl-CH_3CN-5 system. The potentials ranged from −0.15 to −1.35 V with an interval of −0.1 V. (i) Evolution of the real part capacitance vs. frequency for pristine KCl, KCl-DMSO-5, and KCl-CH_3CN-5 electrolyte at −0.45 V.

molecules. Theoretically, the incorporated organic molecule increases the effective radius of solvated K^+, resulting in a decrease in capacitance.[7a] The capacitance was measured using electrochemical impedance spectroscopy, where the real part (C_{re}) of the capacitance represents the EDL capacitance, and the imaginary part reflects irreversible processes such as the electrochemical adsorption of intermediates.[14] As shown in Figure 2i, the recorded C_{re} values are 0.051, 0.045, and 0.021 F cm^{-2} for 0.5 M KCl, KCl-CH_3CN-5, and KCl-DMSO-5, respectively. The significantly reduced EDL capacitance of KCl-DMSO-5 further confirms the successful doping of DMSO molecules into the solvation structure of K^+. To sum up, two different electrolyte systems were constructed, one with (KCl-DMSO-5) and one without (KCl-CH_3CN-5) aprotic organic molecules in the solvation structure.

To assess the influence of molecular-engineered solvation structure on H_2O reduction, we conducted linear sweep voltammetry (LSV) with cathodic scanning using an Ag foil as the working electrode. In an N_2-saturated KCl-DMSO-x electrolyte (where x represents the molar concentration of DMSO), the potential required to attain a current density of 1 mA cm^{-2} ($E_{j=1\ mA\ cm^{-2}}$) shifted negatively from −0.840 to −1.08 V ($\Delta V = 240$ mV) when the DMSO concentration increased from 0 to 8 M (Figure 3a). Potentiostatic electrolysis also showed a gradual decrease in current density at −0.8 V following the addition of DMSO (Figure S5). Online gas chromatography detected only H_2, indicating HER

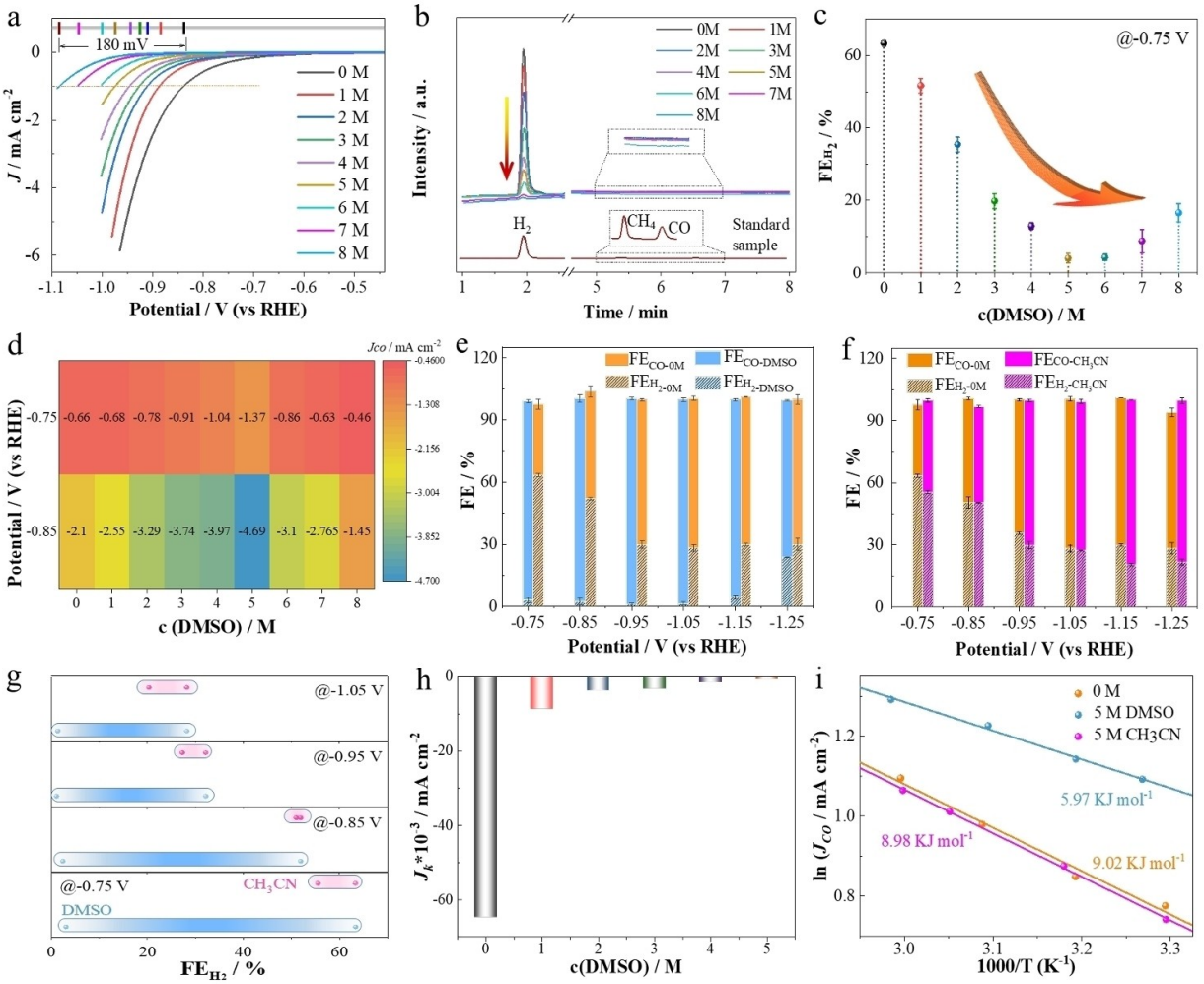

Figure 3. Electrochemical performance. (a) LSV curves of N_2-saturated KCl-DMSO-x. (b) Online gas chromatography analysis of reduction products for N_2-saturated KCl-DMSO-x electrolyte at −0.8 V and the standard sample. The inset is the magnified spectrum within the retention time from 5 to 7 min. (c) H_2 selectivity of the CO_2-saturated KCl-DMSO-x system at −0.75 V. (d) Heatmaps of CO partial current density at −0.75 V and −0.85 V in KCl-DMSO-x electrolyte. FE of H_2 and CO in (e) CO_2-saturated 0.5 M KCl and KCl-DMSO-5, and (f) CO_2-saturated 0.5 M KCl and KCl-CH_3CN-5. (g) Variation of FE_{H2} after adding 5 M DMSO or 5 M CH_3CN in 0.5 M KCl at different potentials. (h) The kinetic current density of HER in KCl-DMSO-x. (i) Arrhenius plots of CO formation over an Ag electrode in 0.5 M KCl, KCl-DMSO-5, and KCl-CH_3CN-5.

is the sole reaction that occurred in this system (Figure 3b). Regarding the hydrogen evolution during CO_2RR, the faradaic efficiency (FE) of H_2 was monitored by varying the amount of DMSO after bubbling CO_2 gas into the electrolyte. In pristine 0.5 M KCl, H_2 is the main reduction product with an FE of 63.32 % at −0.75 V (Figure 3c). However, the FE_{H2} decreased monotonically with the addition of DMSO and reached only 4.01 % in an electrolyte containing 5 M DMSO. Then a slightly increased FE_{H2} is observed for KCl-DMSO-7 and KCl-DMSO-8, even though the FE_{H2} can remain at lower than 10.0 % at −0.85 and −0.95 V (Figure S6). Since only H_2 and CO were detected as end products, the suppressed HER suggests an increased activity for CO_2-to-CO conversion, as evidenced by the variation of the partial current density of CO (J_{CO}, Figure 3d). For example, J_{CO} increased from −2.10 mA cm^{-2} in 0.5 M KCl to −4.69 mA cm^{-2} in DMSO-KCl-5 at −0.85 V, then gradually decreased following the addition of DMSO. The above results suggest the best concentration of DMSO is 5 M. Next, we compared the selectivity of H_2 and CO in 0.5 M KCl and KCl-DMSO-5 from −0.75 to −1.25 V in detail (Figure 3e). The highest CO selectivity was 72.17 % in 0.5 M KCl, consistent with previous reports.[15] Impressively, in KCl-DMSO-5, FE_{CO} of over 90.0 % was achieved within a broad potential window from −0.75 to −1.15 V, culminating with 99.2 % at −0.95 V. DMSO also improved the long-term stability (Figure S7). The electrochemical performance of KCl-CH_3CN-5 was also evaluated for comparison. The LSV curves showed a shift of only 41 mV at $E_{j=1\ mA\ cm^{-2}}$ after introducing 5 M CH_3CN (Figure S8). Selectivity analysis showed the highest FE_{CO} was 79.71 %, very close to the value measured in pure 0.5 M KCl (Figure 3f). The changes in FE_{H2} after the addition of 5 M DMSO and CH_3CN were further compared (Figure 3g). The FE_{H2} in the KCl-DMSO-5 system decreased significantly by 60.25 %, 49.49 %, 31.12 %, and 26.84 % at potentials of −0.75, −0.85, −0.95,

and −1.05 V, respectively. In contrast, the decrease in FE_{H2} in the KCl-CH_3CN-5 system was relatively minimal, with values of 7.85 %, 0.9 %, 4.93 %, and 7.92 % at the same potentials, respectively.

The promoting effect of the organic molecules engineered solvation sheath is strongly associated with the changes in intrinsic activity. In terms of HER, the intrinsic activity can be evaluated using kinetic current density (J_k, Figure S9).[16] As illustrated in Figure 3h, the addition of DMSO in KCl-DMSO-x led to a gradual decrease in J_k, with a remarkable 99.5-fold reduction observed upon increasing DMSO from 0 to 5 M. In contrast, J_k in KCl-CH_3CN-5 reached -55.93×10^{-3} mA cm^{-2} (Figure S10), similar to that in pure 0.5 M KCl (-64.7×10^{-3} mA cm^{-2}). In addition, the electrochemical active surface area (ECSA)-normalized J_{CO} ($J_{CO\text{-}ECSA}$) in KCl-DMSO-5 was found to be higher than that in 0.5 M KCl and KCl-CH_3CN-5 (Figure S11–S12). The apparent activation energies (E_a) for CO_2-to-CO conversion in the three electrolytes were also measured, with values of 9.02, 8.98, and 5.97 kJ mol^{-1} for 0.5 M KCl, KCl-CH_3CN-5, and KCl-DMSO-5, respectively (Figure 3i). Additional validation of the elevated intrinsic CO_2RR activity of KCl-DMSO-5 is demonstrated by microkinetic analysis (Figure S13), which showed a Tafel slope of 161.5 mV dec^{-1} at the low potential region, lower than that of 0.5 M KCl (195.5 mV dec^{-1}) and KCl-CH_3CN-5 (190.1 mV dec^{-1}). These results collectively demonstrate that incorporating DMSO molecules into the solvation shell effectively suppresses the intrinsic activity of HER but boosts the intrinsic activity of CO_2RR, while the presence of freely dispersed CH_3CN in the bulk electrolyte does not have the same effect.

After thoroughly examining potential variations in electrolyte conductivity, composition, electrode surface structure, mass transfer behavior, and interfacial charge transfer resistance (Figure S14–S20), it was concluded that the enhancement in CO_2RR activity within a DMSO-containing electrolyte was not due to any alterations in either the electrolyte or electrode structure and composition. The K^+ also does not play a decisive role in the greatly enhanced CO_2RR activity for the KCl-DMSO-5 system (Figure S21). Instead, our focus shifted to exploring the changes in interfacial H_2O molecules since H_2O is the sole proton source in the system and controls the trade-off between HER and CO_2RR activity. We first mimicked different electrolyte systems (KCl, KCl-DMSO-5, and KCl-CH_3CN-5) by controlling the potential difference between two Ag electrodes, and the adapted simulation setups are shown in Figure 4a–4b and Figure S22.[17] The density distribution of H_2O was calculated as a function of distance from the cathode at a fixed potential of −1.1 V (Figure 4c). All three electrolytes exhibited a first layer within a distance of approximately 3.6 Å in the density profiles, with KCl-DMSO-5 giving the lowest H_2O density of 2.42 g cm^{-3}. The state of H_2O molecules near the electrode was then analyzed by in situ FTIR. According to the deconvolution results of the O–H stretching vibration peaks for KCl-CH_3CN-5 and KCl-DMSO-5 at −0.6 V (Figure 4d and 4e), the H_2O at the interface consists of free H_2O (H_2O–F), H_2O in the hydration shell of cations (coordinated H_2O, H_2O–H), and

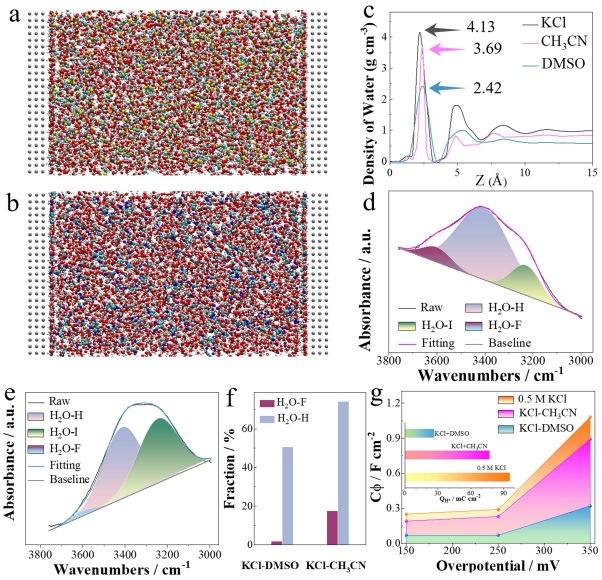

Figure 4. Understanding the changes in interfacial H_2O structure. Snapshots of (a) KCl-DMSO-5, (b) KCl-CH_3CN-5 between two Ag electrodes from MD simulation at −1.1 V, and (c) the corresponding density distribution of H_2O. Deconvolution of the experimental O–H stretching vibration peaks in ATR-FTIR for (d) KCl-CH_3CN-5 and (e) KCl-DMSO-5. (f) Fraction of free H_2O and H_2O in hydration shell for KCl-DMSO-5 and KCl-CH_3CN-5. (g) C_ϕ at various overpotentials for 0.5 M KCl, KCl-CH_3CN-5, and KCl-DMSO-5. Inset shows the corresponding Q_{H^*}.

ice-like H_2O with four hydrogen bonds (H_2O–I). Among them, H_2O–I, being fully bound, cannot pass through IHP;[18] thus, H_2O–F and H_2O–H are considered proton suppliers for HER.[19] The proportion of H_2O–F and H_2O–H was 17.48 % and 74.27 % in KCl-CH_3CN-5, respectively, whereas, in KCl-DMSO-5, only 1.88 % H_2O–F and 50.67 % H_2O–H were observed (Figure 4f). Similar results were obtained at other potentials (Figure S24). The lower availability of proton sources in KCl-DMSO-5 is anticipated to reduce the surface coverage of adsorbed protons (θ_{*H}). This was tested by measuring the hydrogen adsorption charge (Q_{*H}) in N_2-saturated electrolyte, assuming that the change in Q_{*H} matches the change in θ_{*H} because only *H intermediate accounts for the electrochemical response.[20] The integration of overpotential and proton adsorption pseudo-capacitance (C_ϕ) obtained from the imaginary part capacitance in impedance spectroscopy (Figure S25) shows that KCl-DMSO-5 has the lowest Q_{*H} value of 26.5 mC cm^{-2}, while the values for 0.5 M KCl and KCl-CH_3CN-5 are 77 and 95.5 mC cm^{-2}, respectively (Figure 4g). The accumulation of DMSO molecules in EDL reduced the density of H_2O molecules and the relative content of H_2O–F and H_2O–H, resulting in less proton sources and lower surface coverage of *H, thus diminishing the intrinsic activity for HER.

Stabilization and activation of $*H_2O$ steer the kinetic rate of proton-involved steps for CO_2RR, including the formation of *COOH, regardless of the reaction proceeding through coupled or uncoupled proton-electron pathways. To

examine the impact of incorporated DMSO on the stability of *H_2O and other CO_2RR intermediates, in situ SEIRAS was performed by scanning the applied potential negatively from −0.45 to −1.35 V. In the spectra obtained from KCl-DMSO-5 (Figure 5a), the peak ascribed to *CO_2^-, which was the initial one-electron reduction intermediate of CO_2, was identified at 1304 cm^{-1}, in conjunction with a sharp peak of *COOH at 1447 cm^{-1}. Meanwhile, the HCO_3^-, resulting from the chemical equilibrium reaction between dissolved CO_2 and H_2O, was observed at 1447 cm^{-1}. The positive peak at 1653 cm^{-1} is assigned to the H–O–H bending mode of H_2O, which is indicative of the surface-enriched H_2O molecules on the catalyst. These peaks are also observed in the spectra of KCl-CH_3CN-5 and 0.5 M KCl (Figure 5b and S26), indicating that CO_2RR over Ag electrodes in 0.5 M KCl with and without organic additions follows a similar mechanism. The initially adsorbed CO_2 underwent the first electron reduction to form *CO_2^-, which then captured a proton via an H_2O activation process, leading to the formation of *COOH. Subsequently, *CO was generated by an electron and proton transfer step. The absence of the *CO signal in the SEIRAS measurement suggests that CO has facially departed from the Ag electrode.[21]

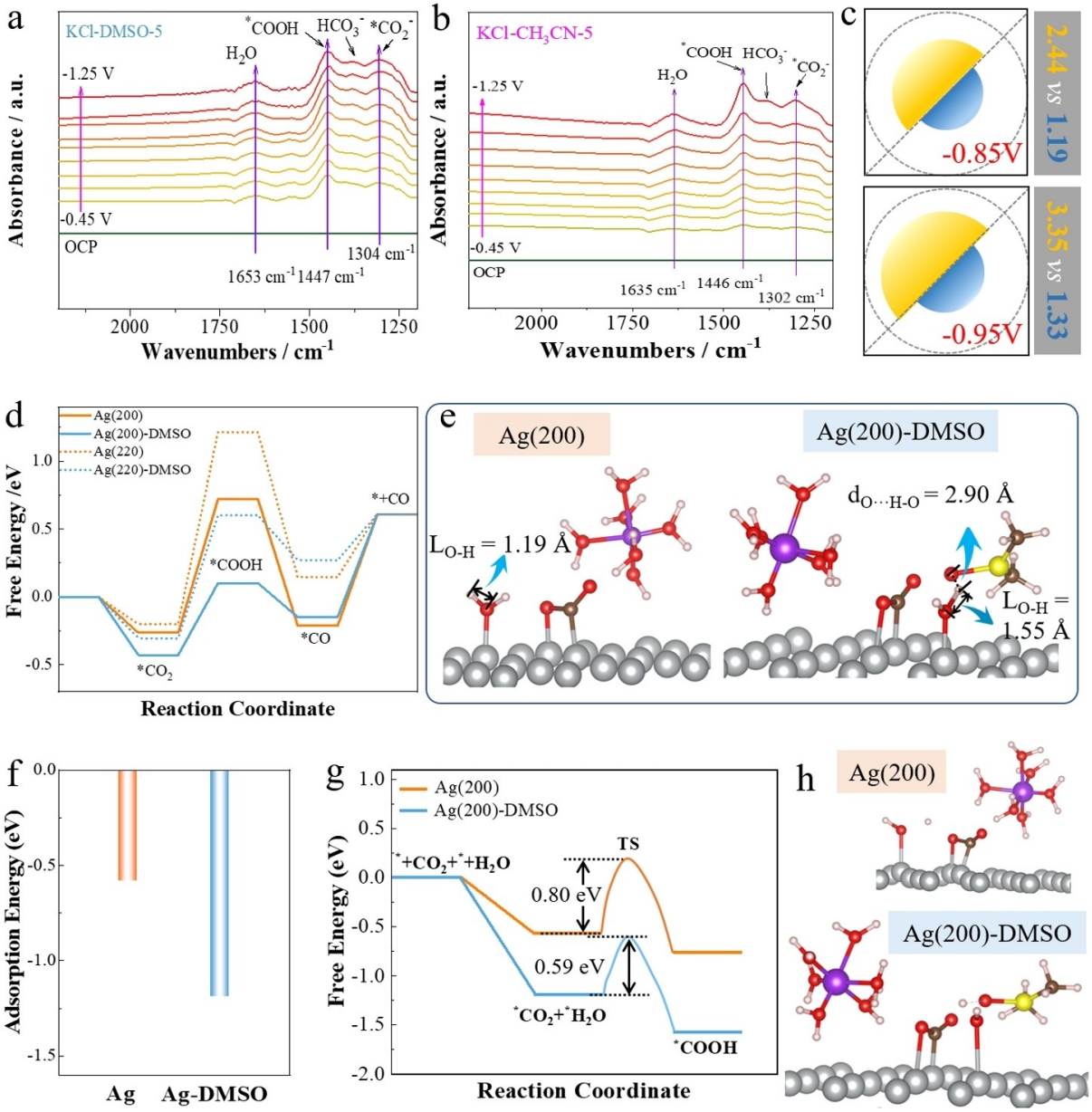

Figure 5. Exploring the enhanced intrinsic activity for CO_2RR. In situ ATR-SEIRAS for (a) KCl-DMSO-5, and (b) KCl-CH_3CN-5. (c) KIE of H/D for CO_2-to-CO conversion at different potentials for KCl-CH_3CN-5 and KCl-DMSO-5. (d) Gibbs free energy changes of CO_2-to-CO conversion over Ag(200) and Ag(220) plane in electrolyte with and without DMSO additive. (e) The models of *CO_2 + *H_2O on Ag(200) and Ag(200)-DMSO sites. (f) The adsorption energy of the H_2O molecule on the Ag site with adsorbed CO_2. (g) Energy barriers of transitional state formation for *CO_2-to-*COOH conversion over Ag electrode in electrolyte with and without DMSO additive. (h) The acquired transitional state models of *CO_2 + H(TS).

The H_2O peak in the KCl-DMSO-5 showed a blue shift to 1653 cm^{-1}, compared to 1635 cm^{-1} in 0.5 M KCl and KCl-CH_3CN-5, indicating the stabilization effect of the regulated solvation structure on the $*H_2O$.[22] This result can be further validated by ATR-SEIRAS collected by reverse potential scan (Figure S27). An analysis of the kinetic isotopic effect (KIE), defined as the ratio of CO generation rate in H_2O- and D_2O-based electrolytes, was performed to assess the impact of DMSO on the proton transfer process for CO_2RR.[23] The KIE values for KCl-CH_3CN-5 were more significant than two at different potentials (Figure 5c), indicating that the rate-determining step involved H_2O dissociation. However, KCl-DMSO-5 had much lower KIE values (1.19 and 1.33 at −0.85 and −0.95 V, respectively), suggesting that the H_2O activation process was significantly accelerated due to the stabilization effect on $*H_2O$. This was further supported by testing the reversible binding behavior of OH^-, which was used as an electrochemical probe to simulate the interaction between $*H_2O$ and organic molecules in the EDL.[24] The potential for OH^- adsorption was found to decrease from 1.86 V in 0.1 M KOH to 1.77 V in KOH-DMSO-5 (Figure S28), while negligible improvement was observed in KOH-CH_3CN-5. These results confirmed that when DMSO is incorporated into the solvation shell of cations, it can interact with $*H_2O$ and enhances $*H_2O$ dissociation.

DFT calculations were also performed to understand the promoting effect of the DMSO-modified solvation environment. As displayed by in situ SEIRAS, the mechanism involving *COOH and *CO intermediates was adopted in the CO_2-to-CO conversion. The models based on Ag (200) and Ag (220) were constructed to represent the interfacial structure of pristine 0.5 M KCl and KCl-CH_3CN-5 (Figure S29), due to the primary crystalline orientation of pristine Ag foil consisting of (200) and (220) facets as shown in the XRD patterns (Figure S15a). A simplified slab composed of an Ag (200) or Ag (220) surface and a complete DMSO molecule was used to relax KCl-DMSO-5 structurally, referred to as Ag-DMSO (Figure S30). A solvated K^+ was also introduced during the calculations.[2a] The free energy plot in Figure 5d showed that the reduction of CO_2 to CO over the Ag(200) was dominated by the formation of *COOH with a ΔG of 0.99 eV, and the energy barrier of this step was reduced to 0.53 eV with the addition of a DMSO molecule. Meanwhile, the calculated ΔG of *CO desorption was found to be similar for both Ag and Ag-DMSO, indicating that the presence of DMSO did not affect this step. This result intuitively contradicts the linear scaling relationship between the adsorption energy of *COOH and *CO.[25] A similar conclusion can be achieved for Ag (220) system. Therefore, the greatly accelerated formation of *COOH is not due to the direct interaction between *COOH and the DMSO molecule. This is confirmed by the observation of identical wavenumbers in the in situ SEIRAS for the *COOH peaks in both electrolytes with and without organic additives (Figures 5a and 5b).

Next, we gain insight into the formation process of *COOH, namely the protonation of $*CO_2$, by considering the adsorption and activation of the H_2O molecule. Firstly, the adsorption energy of the H_2O molecule was calculated at the Ag site with adsorbed CO_2. As presented in Figure 5e, the adsorption configuration model of $*CO_2 + *H_2O$ clearly shows the interaction between the S=O moiety in DMSO and the H–O group in H_2O. The distance of O···H–O (d) was 2.09 Å, which is in the range of the classical H-bond interaction.[26] This interaction is also evident from the blue shift of the bending vibration peak of H_2O in FTIR spectra of KCl-DMSO-5,[27] as discussed above. In particular, the H-bond interaction lengthened the O–H bond from 1.19 Å to 1.55 Å, illustrating the weakened bond strength of the O–H bond and could accelerate the activation of $*H_2O$ ($H_2O + e^- + * \rightarrow *H + OH^-$). Therefore, the adsorption energy of H_2O decreased from −0.58 eV (Ag(200)) to −1.19 eV (Ag(200)-DMSO) (Figure 5f). Second, the energy changes of $*H_2O$ activation and subsequent $*CO_2$ protonation were evaluated for both Ag(200) and Ag(200)-DMSO models. As shown in Figure 5g, starting from the initial state of $*CO_2 + *H_2O$, the *COOH was generated after H_2O activation. After searching for transition states, the optimized state of $*CO_2 + H(TS)$ was built, and an apparent stabilization effect of DMSO on the generated proton was observed in Ag-DMSO via S=O···H interaction (Figure 5h). Finally, the ΔG for the conversion of $*CO_2$ to *COOH reduced from 0.80 eV (Ag(200)) to 0.59 eV (Ag(200)-DMSO). These results explain well the improved CO_2RR intrinsic activity in KCl-DMSO-5.

The versatility of this strategy could be validated with different electrodes and aprotic organic molecule additives (Figure S37–S42). The CO selectivity over Zn foil in KCl-DMSO-5 is higher than the pristine KCl electrolyte at all potentials, with the largest improvement of 29.3 % at −0.75 V and the highest FE_{CO} of 84.05 %, better than other Zn foil electrodes.[28] Considering the higher Gutmann donor number of N,N-dimethylformamide (DMF, 26.6) than H_2O, the solvation structure and corresponding CO_2RR activity of KCl-DMF-5 were also analyzed. MD simulation showed a K–O distance of 2.63 Å, which is comparable to $K\text{-}O_{water}$ pair (Figure S39b). The density profile of H_2O at −1.1 V also demonstrated the enrichment of DMF near the cathode (Figure S40). Electrochemical tests showed improved CO selectivity of the Ag electrode when DMF was introduced (Figure S41), with the highest FE_{CO} increasing from 72.17 % in 0.5 M KCl to 90.25 % in KCl-DMF-5. The improvement in CO_2 reduction selectivity was also observed for CO_2-to-formate conversion over the Sn electrode in the KCl-DMF-5 electrolyte (Figure S42), with DMF molecules suppressing HER but boosting FE_{CO} and $FE_{formate}$. Notably, the highest $FE_{formate}$ reached 91.57 %, which was superior to the pure KCl electrolyte (77.77 %).

Conclusion

In summary, a molecular engineering strategy was proposed to balance H_2O activation for HER and CO_2RR by modifying the solvation structure of metal cations. This strategy involves incorporating aprotic organic molecules with higher Gutmann donor numbers than H_2O into the

solvation shell of electrolyte cations. The results of MD simulations and in situ ATR-SEIRAS experiments, utilizing DMSO as a representative molecule, demonstrated the capability of these molecules to enter the solvation shell of K^+ and incrementally concentrate within the EDL under an electric field. The locally enriched DMSO reduced the density of H_2O molecules at the interface from 4.13 $g\,cm^{-3}$ in pure KCl electrolyte to 2.42 $g\,cm^{-3}$ in KCl-DMSO-5. The significant reduction in the proportion of two proton sources, H_2O–F and H_2O–H, results in a lower surface coverage of H* and a decreased inherent activity of the HER process. The selectivity of H_2 production over the Ag electrode at −0.75 V dropped dramatically, from 63.32 % in 0.5 M KCl to 4.01 %, upon the addition of 5 M DMSO. This also resulted in a 99.5-fold reduction in the J_k value. In addition, the presence of DMSO was observed to stabilize $*H_2O$ and accelerate the protonation of $*CO_2$ involving a transition state of $*CO_2+H$(TS) with an energy barrier of 0.59 eV, much lower than that of the original Ag electrode (0.80 eV). The intrinsic activity for CO_2RR was significantly enhanced, as demonstrated by the decrease in the free energy change for the *COOH formation and the measured apparent activation energy. Notably, this approach disrupts the linear scaling relationship between the adsorption strength of *COOH and *CO because the incorporated DMSO molecules do not interact directly with these intermediates. As a result, an optimized activation of H_2O was realized by constructing a DMSO-incorporated EDL. Finally, a CO selectivity of over 90 % can be achieved in KCl-DMSO-5 from −0.75 to −1.15 V, with a peak FE_{CO} value of 99.2 % at −0.95 V. These findings have also been observed for other electrodes, such as Zn and Sn, as well as other organic molecules, like DMF. The versatility of organic molecules allows for fine-tuning of the solvation layer of electrolyte cations, providing significant potential for the design of effective electrocatalysts for CO_2RR and other electrochemical reactions.

Acknowledgements

This work was financially supported by the Intergovernmental International Science and Technology Innovation Cooperation Program of the National Key Research and Development Program (Grant No. 2022YFE0120200), the National Natural Science Foundation of China (Grant No. 21872046, 52072118, and 52102041), the Jiebang Guashuai Project of Hunan Province (Grant No. 2021GK1110), the Research and Development Plan of Key Areas in Hunan Province (Grant No. 2019GK2235), and the Natural Science Foundation of Hunan Province (Grant No. 2020JJ4174, 2022JJ40073).

Conflict of Interest

The authors declare no conflict of interest.

Data Availability Statement

The data that support the findings of this study are available in the supplementary material of this article.

Keywords: CO_2 Electroreduction · H_2O Activation · Molecular Engineering · Solvation Structure

[1] M. B. Ross, P. De Luna, Y. F. Li, C. T. Dinh, D. Kim, P. Yang, E. H. Sargent, *Nat. Catal.* **2019**, *2*, 648–658.

[2] a) Y. R. Wang, M. Liu, G. K. Gao, Y. L. Yang, R. X. Yang, H. M. Ding, Y. F. Chen, S. L. Li, Y. Q. Lan, *Angew. Chem. Int. Ed.* **2021**, *60*, 21952–21958; b) J. Y. Chen, Z. J. Li, X. Y. Wang, X. H. Sang, S. X. Zheng, S. J. Liu, B. Yang, Q. H. Zhang, L. C. Lei, L. M. Dai, Y. Hou, *Angew. Chem. Int. Ed.* **2022**, *61*, e202111683; c) S. H. Chen, Z. D. Zhang, W. J. Jiang, S. S. Zhang, J. X. Zhu, L. Q. Wang, H. H. Ou, S. Zaman, L. Tan, P. Zhu, E. R. Zhang, P. Jiang, Y. Q. Su, D. S. Wang, Y. D. Li, *J. Am. Chem. Soc.* **2022**, *144*, 12807–12815; d) Z. S. Han, D. L. Han, Z. Chen, J. C. Gao, G. Y. Jiang, X. Y. Wang, S. S. Lyu, Y. Guo, C. N. Geng, L. C. Yin, Z. Weng, Q. H. Yang, *Nat. Commun.* **2022**, *13*, 3158–3167.

[3] a) S. J. Shin, H. Choi, S. Ringe, D. H. Won, H. S. Oh, D. H. Kim, T. Lee, D. H. Nam, H. Kim, C. H. Choi, *Nat. Commun.* **2022**, *13*, 5482–5491; b) M. R. Singh, Y. Kwon, Y. Lum, J. W. Ager, A. T. Bell, *J. Am. Chem. Soc.* **2016**, *138*, 13006–13012; c) L. D. Chen, M. Urushihara, K. R. Chan, J. K. Norskov, *ACS Catal.* **2016**, *6*, 7133–7139; d) F. Zhang, A. C. Co, *Angew. Chem. Int. Ed.* **2020**, *59*, 1674–1681; e) V. Sinha, E. Khramenkova, E. A. Pidko, *Chem. Sci.* **2022**, *13*, 3803–3808; f) A. N. Xu, N. Govindarajan, G. Kastlunger, S. Vijay, K. R. Chan, *Acc. Chem. Res.* **2022**, *55*, 495–503; g) J. Y. Li, X. Li, C. M. Gunathunge, M. M. Waegele, *Proc. Natl. Acad. Sci. USA* **2019**, *116*, 9220–9229; h) M. König, J. Vaes, E. Klemm, D. Pant, *iScience* **2019**, *19*, 135–160; i) D. F. Gao, R. M. Aran-Ais, H. S. Jeon, B. Roldan Cuenya, *Nat. Catal.* **2019**, *2*, 198–210; j) J. C. Bui, C. Kim, A. J. King, O. Romiluyi, A. Kusoglu, A. Z. Weber, A. T. Bell, *Acc. Chem. Res.* **2022**, *55*, 484–494.

[4] a) S. Banerjee, C. S. Gerke, V. S. Thoi, *Acc. Chem. Res.* **2022**, *55*, 504–515; b) A. S. Malkani, J. Li, N. J. Oliveira, M. He, X. Chang, B. Xu, Q. Lu, *Sci. Adv.* **2020**, *6*, 2569–2580; c) B. W. Deng, M. Huang, X. L. Zhao, S. Y. Mou, F. Dong, *ACS Catal.* **2022**, *12*, 331–362; d) M. F. Delley, E. M. Nichols, J. M. Mayer, *J. Phys. Chem. C* **2022**, *126*, 8477–8488.

[5] a) Y. Zhong, Y. Xu, J. Ma, C. Wang, S. Sheng, C. Cheng, M. Li, L. Han, L. Zhou, Z. Cai, Y. Kuang, Z. Liang, X. Sun, *Angew. Chem. Int. Ed.* **2020**, *59*, 19095–19101; b) A. S. Varela, W. Ju, T. Reier, P. Strasser, *ACS Catal.* **2016**, *6*, 2136–2144; c) T. H. Yuan, T. Wang, G. Zhang, W. Y. Deng, D. F. Cheng, H. Gao, J. Zhao, J. Yu, P. Zhang, J. L. Gong, *Chem. Sci.* **2022**, *13*, 8117–8123; d) W. X. Ge, Y. X. Chen, Y. Fan, Y. H. Zhu, H. L. Liu, L. Song, Z. Liu, C. Lian, H. L. Jiang, C. Z. Li, *J. Am. Chem. Soc.* **2022**, *144*, 6613–6622; e) S. Banerjee, X. Han, V. S. Thoi, *ACS Catal.* **2019**, *9*, 5631–5637.

[6] C. X. Zhao, Y. F. Bu, W. Gao, Q. Jiang, *J. Phys. Chem. C* **2017**, *121*, 19767–19773.

[7] a) S. Ringe, E. L. Clark, J. Resasco, A. Walton, B. Seger, A. T. Bell, K. Chan, *Energy Environ. Sci.* **2019**, *12*, 3001–3014; b) J. A. Rebstock, Q. S. Zhu, L. R. Baker, *Chem. Sci.* **2022**, *13*, 7634–7643; c) J. Resasco, L. D. Chen, E. Clark, C. Tsai, C. Hahn, T. F. Jaramillo, K. Chan, A. T. Bell, *J. Am. Chem. Soc.* **2017**, *139*, 11277–11287.

[8] J. Gu, S. Liu, W. Y. Ni, W. H. Ren, S. Haussener, X. L. Hu, *Nat. Catal.* **2022**, *5*, 268–276.

[9] a) Q. Dong, X. Z. Zhang, D. He, C. C. Lang, D. W. Wang, *ACS Cent. Sci.* **2019**, *5*, 1461–1467; b) W. Ren, A. Xu, K. Chan, X. Hu, *Angew. Chem. Int. Ed.* **2022**, *61*, e202214173.
[10] M. C. O. Monteiro, F. Dattila, N. Lopez, M. T. M. Koper, *J. Am. Chem. Soc.* **2022**, *144*, 1589–1602.
[11] G. Senanayake, D. M. Muir, *Metall. Trans. B* **1990**, *21*, 439–448.
[12] F. Cataldo, *Eur. Chem. Bull.* **2015**, *4*, 92–97.
[13] M. Dunwell, Y. S. Yan, B. J. Xu, *Surf. Sci.* **2016**, *650*, 51–56.
[14] J. B. Zhu, Y. L. Xu, J. Wang, J. Lin, X. F. Sun, S. C. Mao, *Phys. Chem. Chem. Phys.* **2015**, *17*, 28666–28673.
[15] a) W. Y. Deng, L. Zhang, H. Dong, X. X. Chang, T. Wang, J. L. Gong, *Chem. Sci.* **2018**, *9*, 6599–6604; b) M. S. Jee, H. S. Jeon, C. Kim, H. Lee, J. H. Koh, J. Cho, B. K. Min, Y. J. Hwang, *Appl. Catal. B* **2016**, *180*, 372–378; c) A. Thevenon, A. Rosas-Hernandez, A. M. F. Herreros, T. Agapie, J. C. Peters, *ACS Catal.* **2021**, *11*, 4530–4537.
[16] a) R. He, A. Zhang, Y. L. Ding, T. Y. Kong, Q. Xiao, H. L. Li, Y. Liu, J. Zeng, *Adv. Mater.* **2018**, *30*, 1705872–1705878; b) W. P. Ni, Z. X. Liu, X. G. Guo, Y. Zhang, C. Ma, Y. J. Deng, S. G. Zhang, *Appl. Catal. B* **2021**, *291*, 120092–120101.
[17] J. Vatamanu, O. Borodin, G. D. Smith, *J. Phys. Chem. C* **2012**, *116*, 1114–1121.
[18] a) Q. L. Wen, J. Y. Duan, W. B. Wang, D. J. Huang, Y. W. Liu, Y. L. Shi, J. K. Fang, A. M. Nie, H. Q. Li, T. Y. Zhai, *Angew. Chem. Int. Ed.* **2022**, *61*, e202206077; b) D. Strmcnik, M. Escudero-Escribano, K. Kodama, V. R. Stamenkovic, A. Cuesta, N. M. Markovic, *Nat. Chem.* **2010**, *2*, 880–885.
[19] a) F. H. Yang, J. A. Yuwono, J. N. Hao, J. Long, L. B. Yuan, Y. Y. Wang, S. L. Liu, Y. M. Fan, S. Y. Zhao, K. Davey, Z. P. Guo, *Adv. Mater.* **2022**, *34*, 2206754; b) P. Li, Y. L. Jiang, Y. C. Hu, Y. N. Men, Y. W. Liu, W. B. Cai, S. L. Chen, *Nat. Catal.* **2022**, *5*, 900–911.
[20] J. D. Chen, C. H. Chen, M. K. Qin, B. Li, B. B. Lin, Q. Mao, H. B. Yang, B. Liu, Y. Wang, *Nat. Commun.* **2022**, *13*, 5382–5391.
[21] a) S. B. Liu, H. B. Tao, L. Zeng, Q. Liu, Z. G. Xu, Q. X. Liu, J. L. Luo, *J. Am. Chem. Soc.* **2017**, *139*, 2160–2163; b) K. Ye, T. F. Liu, Y. P. Song, Q. Wang, G. X. Wang, *Appl. Catal. B* **2021**, *296*, 120342–120349; c) Z. Zhang, G. B. Wen, D. Luo, B. H. Ren, Y. F. Zhu, R. Gao, H. Z. Dou, G. R. Sun, M. Feng, Z. Y. Bai, A. P. Yu, Z. W. Chen, *J. Am. Chem. Soc.* **2021**, *143*, 6855–6864.
[22] K. Lakshmanan, W. H. Huang, S. A. Chala, B. W. Taklu, E. A. Moges, J. F. Lee, P. Y. Huang, Y. C. Lee, M. C. Tsai, W. N. Su, B. J. Hwang, *Adv. Funct. Mater.* **2022**, *32*, 2109310–2109319.
[23] Y. H. Lin, C. Y. Deng, L. Wu, Y. C. Zhang, C. C. Chen, W. H. Ma, J. C. Zhao, *Energy Environ. Sci.* **2020**, *13*, 2602–2617.
[24] S. Mukhopadhyay, R. Shimoni, I. Liberman, R. Ifraemov, I. Rozenberg, I. Hod, *Angew. Chem. Int. Ed.* **2021**, *60*, 13423–13429.
[25] X. Hong, K. R. Chan, C. Tsai, J. K. Norskov, *ACS Catal.* **2016**, *6*, 4428–4437.
[26] T. Steiner, *Angew. Chem. Int. Ed.* **2002**, *41*, 48–76.
[27] S. O. Paul, T. A. Ford, *J. Crystallogr. Spectrosc. Res.* **1986**, *16*, 811–821.
[28] a) D. L. T. Nguyen, M. S. Jee, D. H. Won, H. Jung, H. S. Oh, B. K. Min, Y. J. Hwang, *ACS Sustainable Chem. Eng.* **2017**, *5*, 11377–11386; b) T. L. Chen, H. C. Chen, Y. P. Huang, S. C. Lin, C. H. Hou, H. Y. Tan, C. W. Tung, T. S. Chan, J. J. Shyue, H. M. Chen, *Nanoscale* **2020**, *12*, 18013–18021; c) W. Luo, J. Zhang, M. Li, A. Zuttel, *ACS Catal.* **2019**, *9*, 3783–3791; d) H. S. Jeon, I. Sinev, F. Scholten, N. J. Divins, I. Zegkinoglou, L. Pielsticker, B. Roldan Cuenya, *J. Am. Chem. Soc.* **2018**, *140*, 9383–9386.

Manuscript received: March 3, 2023
Accepted manuscript online: July 28, 2023
Version of record online: August 4, 2023